Crystal structure and phase transitions across the metal-superconductor boundary in the $SmFeAsO_{1-x}F_x$ ($0 \leq x \leq 0.20$) family

Serena Margadonna,[1,*] Yasuhiro Takabayashi,[2] Martin T. McDonald,[2] Michela Brunelli,[3] G. Wu,[4] R. H. Liu,[4] X. H. Chen,[4] and Kosmas Prassides[2,*]

[1]*School of Chemistry, University of Edinburgh, Edinburgh EH9 3JJ, United Kingdom*

[2]*Department of Chemistry, University of Durham, Durham DH1 3LE, United Kingdom*

[3]*European Synchrotron Radiation Facility, 38042 Grenoble, France*

[4]*Hefei National Laboratory for Physical Science at Microscale and Department of Physics, University of Science and Technology of China, Hefei, Anhui 230026, China*

(Received 1 December 2008; published 6 January 2009)

The fluorine-doped rare-earth iron oxyarsenides $REFeAsO_{1-x}F_x$ (RE=rare earth) have recently emerged as a new family of high-temperature superconductors with transition temperatures (T_c) as high as 55 K. Here we use high-resolution synchrotron x-ray diffraction to study the structural properties of $SmFeAsO_{1-x}F_x$ ($0 \leq x \leq 0.20$) in which superconductivity emerges near $x \sim 0.07$ and T_c increases monotonically with doping up to $x \sim 0.20$. We find that orthorhombic symmetry survives through the metal-superconductor boundary well into the superconducting regime and the structural distortion is only suppressed at doping levels, $x \geq 0.15$, when the superconducting phase becomes metrically tetragonal. Remarkably this crystal symmetry crossover coincides with reported drastic anomalies in the resistivity and the Hall coefficient, and a switch of the pressure coefficient of T_c from positive to negative, thereby implying that the low-temperature structure plays a key role in defining the electronic properties of these superconductors.

DOI: 10.1103/PhysRevB.79.014503 PACS number(s): 74.70.Dd, 61.05.C−, 74.25.Ha

I. INTRODUCTION

The possible mechanism of superconductivity in the $REFeAsO_{1-x}F_x$ (RE=La, Ce, Pr, Nd, Sm, and Gd) and related $REFeAsO_{1-\delta}$ materials is currently unknown.[1–6] The rapidly developing structural and electronic phenomenologies[7–10] point to considerable similarities with the well-established behavior of high-T_c cuprate superconductors, and early theoretical work has suggested that conventional electron-phonon coupling mechanisms are not able to account for the high T_c, implying non-BCS origin of the pairing interactions.[11–14] Nonetheless, a single superconducting gap $2\Delta = 13.3(3)$ meV exhibiting a BCS-type temperature dependence has been reported for the 42 K $SmFeAsO_{0.85}F_{0.15}$ superconductor.[15] Early experimental work has also provided compelling evidence that the undoped REFeAsO parent materials exhibit spin-density-wave (SDW) antiferromagnetic order and undergo a structural phase transition from tetragonal-to-orthorhombic crystal symmetry upon cooling.[7,9,16] This is strongly reminiscent of the behavior of the parent cuprate phase, La_2CuO_4. Upon doping with fluoride ions, again much like $La_{2-x}Sr_xCuO_4$, both the crystallographic and magnetic transitions are suppressed in the $REFeAsO_{1-x}F_x$ superconducting compositions[8,9] while T_c first increases smoothly before passing over a maximum value at an optimal level of doping.[3,4,10] Detailed experimental mapping of the structural and electronic phase diagrams as the doping level x varies is necessary before we achieve a fundamental understanding of the superconductivity mechanism.

Here we probed the temperature evolution of the structural properties of the $SmFeAsO_{1-x}F_x$ ($0 \leq x \leq 0.20$) family by high-resolution synchrotron x-ray powder diffraction between 20 and 295 K. We find that the crystal symmetry at low temperatures is orthorhombic for the nonsuperconducting compositions when SDW antiferromagnetic order is present ($x < 0.07$). However, unlike the long-range magnetic order,[8,9] the tetragonal-to-orthorhombic structural transition is not suppressed as we cross into the superconducting regime with the orthorhombic distortion being present for compositions with $x \leq 0.12$ and disappearing only at higher doping levels ($x \geq 0.15$). Although there is no accompanying discontinuity in the doping level dependence of T_c, the difference in crystal symmetry of the superconducting state is clearly reflected in the electronic properties of the superconducting phases.

II. EXPERIMENTAL DETAILS

Polycrystalline samples with nominal composition $SmFeAsO_{1-x}F_x$ (x=0, 0.05, 0.10, 0.12, 0.15, and 0.20) were synthesized by conventional solid-state reactions using high-purity SmAs, SmF_3, Fe, and Fe_2O_3, as described elsewhere.[2,10,17] The samples were characterized by powder x-ray diffraction, and temperature-dependent resistivity and dc magnetization measurements. Bulk superconductivity is observed for x=0.10 at ~17 K. T_c increases monotonically with increasing F^- content and reaches a maximum value of ~54 (from resistivity measurements[10]) or ~49 K (from magnetization measurements[17]) at the optimal doping, x=0.20. For the synchrotron x-ray diffraction measurements, the $SmFeAsO_{1-x}F_x$ ($0 \leq x \leq 0.20$) samples were sealed in thin-walled glass capillaries 0.5 mm in diameter. With each sample inside a continuous-flow cryostat, high-statistic synchrotron x-ray powder-diffraction data (λ=0.399 861 Å, $2\theta = 1° - 50°$, d spacing=22.85–0.47 Å) were collected at 20 and 200 K in continuous scanning mode with the high-resolution multianalyzer powder diffractometer on beamline

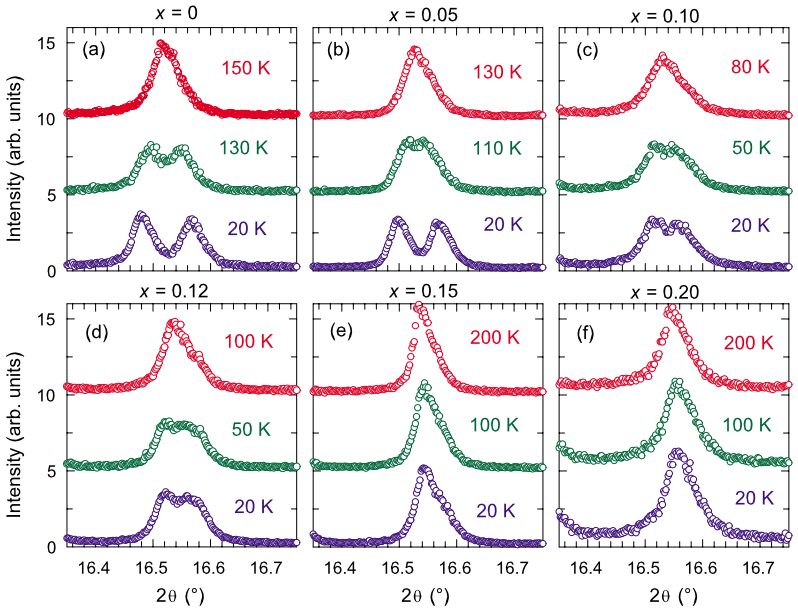

FIG. 1. (Color online) Selected region of the high-resolution synchrotron x-ray powder-diffraction profiles of $SmFeAsO_{1-x}F_x$ showing the temperature evolution of the $(220)_T$ Bragg reflection ($\lambda=0.399\,86$ Å). (a) $x=0$, (b) $x=0.05$, (c) $x=0.10$, (d) $x=0.12$, (e) $x=0.15$, and (f) $x=0.20$. On cooling, the tetragonal peak splits into a doublet $[(040)_O, (400)_O]$ for $x=0-0.12$ while no detectable splitting is found for $x=0.15$ and 0.20 even at the ultrahigh resolution of the present data. The width of the $(220)_T$ reflection for $x=0$, 0.05, and 0.10 begins to increase before the onset of the tetragonal-to-orthorhombic structural transition (at 150, 130, and 75 K, respectively) providing the signature of precursor strain effects associated with the development of local structural inhomogeneities. No change in the width of reflections [e.g., $(102)_T$] that do not split through the structural transition is observed.

ID31 at the European Synchrotron Radiation Facility (ESRF), Grenoble, France. Lower statistic diffraction profiles were also recorded on cooling at numerous temperatures between 295 and 20 K over a shorter angular range ($2\theta=1°-40°$, d spacing$=22.85-0.59$ Å). Data analysis was performed with the GSAS suite of Rietveld analysis programs.[18]

III. RESULTS

Inspection of all diffraction profiles at room temperature readily reveals the tetragonal (T) unit cell (space-group $P4/nmm$) established before for other REFeAsO systems.[7,16] Therefore all the $SmFeAsO_{1-x}F_x$ compositions studied here are isostructural and adopt the layered ZrCuSiAs-type structure, featuring alternating tetrahedrally coordinated Sm-(O/F) and Fe-As layers along the crystallographic c axis. Rietveld analysis of the room-temperature diffraction profiles proceeded smoothly for all compositions, revealing a monotonic decrease in both lattice constants with increasing doping level, x [at 295 K—$SmFeAsO$: $a_T=3.938\,80(2)$ Å, $c_T=8.511\,11(7)$ Å (reliability R factors: $R_{wp}=5.26\%$, $R_{\rm exp}=3.31\%$); $SmFeAsO_{0.90}F_{0.10}$: $a_T=3.936\,68(2)$ Å, $c_T=8.493\,29(6)$ Å ($R_{wp}=4.83\%$, $R_{\rm exp}=2.61\%$); $SmFeAsO_{0.80}F_{0.20}$: $a_T=3.932\,54(4)$ Å, $c_T=8.484\,2(1)$ Å ($R_{wp}=8.27\%$, $R_{\rm exp}=5.86\%$)].[19] The response of the lattice metrics to F^- substitution is strongly anisotropic with the interlayer spacing showing a significantly larger contraction than the intralayer dimensions with increasing x ($\partial \ln c_T/\partial x \sim 1.6\times10^{-2}$, $\partial \ln a_T/\partial x \sim 0.8\times10^{-2}$).

However, the observed structural behavior of the various $SmFeAsO_{1-x}F_x$ compositions is very different on cooling. No

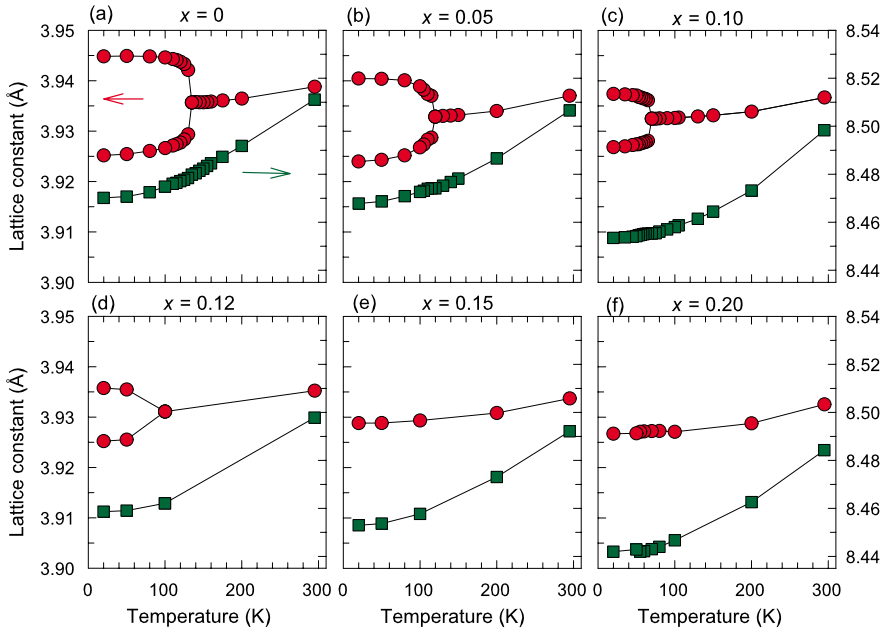

FIG. 2. (Color online) Temperature evolution of the structural parameters of the $SmFeAsO_{1-x}F_x$ family. (a) $x=0$, (b) $x=0.05$, (c) $x=0.10$, (d) $x=0.12$, (e) $x=0.15$, and (f) $x=0.20$. Squares label the interlayer c lattice constant (right scale). Circles label the in-plane a and b lattice constants (left scale). In (a)–(d), the a and b lattice constants are divided by $\sqrt{2}$ at temperatures below the tetragonal-to-orthorhombic transition, T_s. Error bars are smaller than the size of the symbols.

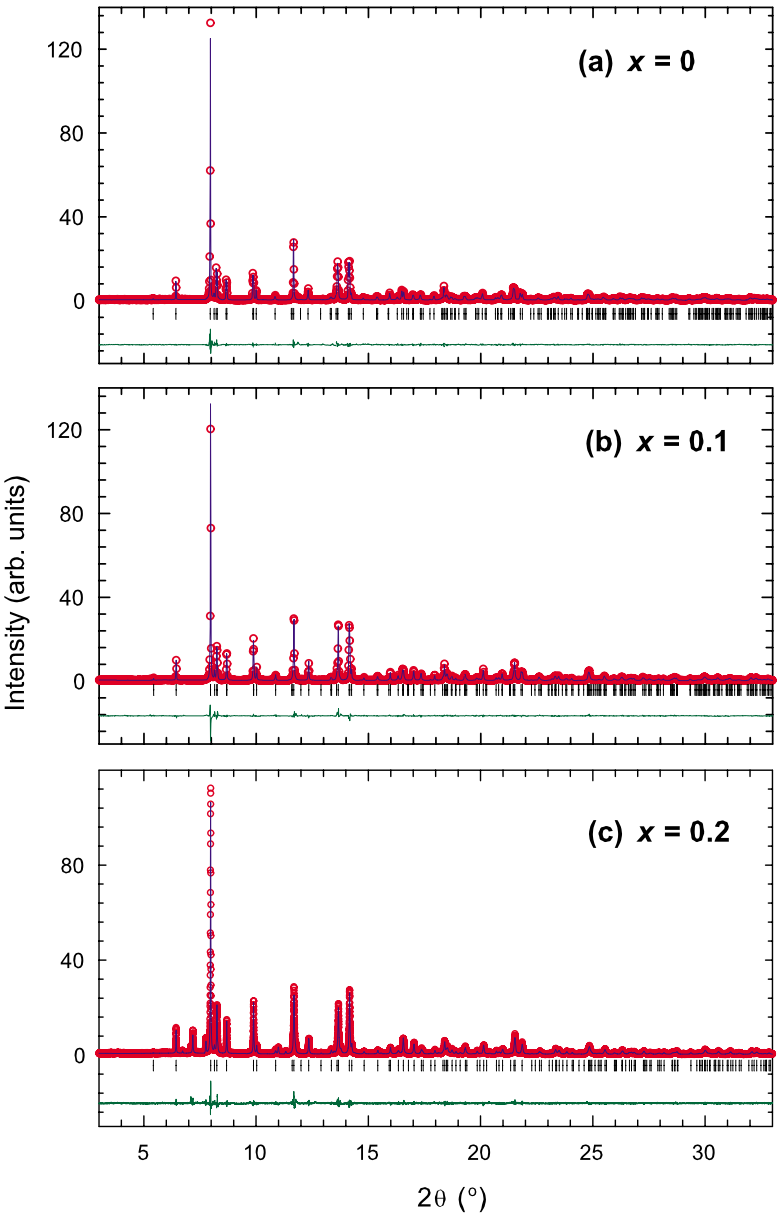

FIG. 3. (Color online) Final observed (red circles) and calculated (blue solid line) synchrotron x-ray (λ=0.399 861 Å) powder-diffraction profiles at 20 K for the $SmFeAsO_{1-x}F_x$ samples with (a) x=0, (b) x=0.1, and (c) x=0.2. The lower green solid lines show the difference profile and the tick marks show the reflection positions of the orthorhombic (x=0 and 0.1) and tetragonal (x=0.2) phases, respectively. The corresponding results for the compositions with x=0.054, 0.12, and 0.15 are included in the accompanying supplementary information (Ref. 19).

reflections violating tetragonal extinction rules are evident for the heavily doped compositions with x=0.15 and 0.20 [Figs. 1(e) and 1(f)], in which both lattice constants a and c decrease smoothly with their crystal structure remaining strictly tetragonal down to 20 K [Figs. 2(e) and 2(f)]. The rate of contraction, $d \ln a/dT$ and $d \ln c/dT$, at ~5 and ~18 ppm K^{-1} for the a and c lattice constants, respectively, is considerably anisotropic and leads to a gradual decrease in the (c/a) ratio with decreasing temperature. This behavior is in sharp contrast to the observed thermal structural response of the $SmFeAsO_{1-x}F_x$ (x=0, 0.05, 0.10, and 0.12) compositions. In these systems, the tetragonal structure is initially robust upon cooling, showing a normal contraction of the lattice parameters and interatomic distances. However, as the samples are cooled further, the (hkl) $(h,k \neq 0)$ reflections in the diffraction profiles begin first to broaden before splitting at a characteristic temperature, T_s [Figs. 1(a)–1(d)], thereby providing the signature of the onset of a structural transformation of the high-temperature tetragonal structure.[7,16] Rietveld refinements of the low-temperature diffraction profiles confirm the adoption of the same orthorhombic (O) superstructure of lattice dimensions, $b_O > a_O \sim a_T\sqrt{2}$ and $c_O \sim c_T$ (space group $Cmma$) for all $0 \leq x \leq 0.12$ compositions [Figs. 2(a)–2(d)]. Representative refined lattice constants at 20 K are: SmFeAsO, a_O=5.551 05(5) Å, b_O=5.578 84(5) Å, c_O =8.470 14(9) Å (reliability R factors: R_{wp}=7.90%, $R_{\rm exp}$ =6.11%); $SmFeAsO_{0.90}F_{0.10}$, a_O=5.553 39(5) Å, b_O =5.568 29(5) Å, c_O=8.453 45(6) Å (R_{wp}=7.17%, $R_{\rm exp}$ =5.70%) (Fig. 3, Table I).[19] No discontinuity is observed at T_s in the thermal response of either the lattice constant c or the normalized unit-cell volume V. Notably as the doping level x increases, both the transition temperature T_s (130 K for x=0, 115 K for x=0.05, 65 K for x=0.10, and 50 K for x=0.12) and the magnitude of the orthorhombic strain coefficient $s=(b_O-a_O)/(b_O+a_O)$ ($\sim 2.5 \times 10^{-3}$ at 20 K for x=0 to $\sim 1.1 \times 10^{-3} - 1.3 \times 10^{-3}$ at 20 K for x=0.10 and 0.12) decrease smoothly.

TABLE I. Refined lattice constants, atomic parameters, and selected bond lengths (Å) and angles (°) at 20 K for $SmFeAsO_{1-x}F_x$ (x=0, 0.05, 0.1, 0.12, 0.15, and 0.2) from the Rietveld refinements of the synchrotron x-ray powder-diffraction profiles. Estimated errors in the last digits are given in parentheses. The temperature factors of O and F were constrained to be equal, and the sum of the fractional occupancies of O and F was constrained to be equal to one. Rietveld refinements proceeded smoothly for all compositions using profile function number 3 of the GSAS Rietveld refinement program (Ref. 18) that incorporates an empirical expression for microstrain anisotropy which is present when the sample contains stacking faults that will selectively broaden some reflections.

	SmFeAsO	$SmFeAsO_{0.95}F_{0.05}$	$SmFeAsO_{0.9}F_{0.1}$	$SmFeAsO_{0.88}F_{0.12}$	$SmFeAsO_{0.85}F_{0.15}$	$SmFeAsO_{0.8}F_{0.2}$
Space group	*Cmma* [a]	*Cmma* [a]	*Cmma* [a]	*Cmma* [a]	*P*4/*nmm* [b]	*P*4/*nmm* [b]
a (Å)	5.551 05(5)	5.549 36(4)	5.553 39(5)	5.551 10(5)	3.928 91(2)	3.926 99(3)
b (Å)	5.578 84(5)	5.572 63(4)	5.568 29(5)	5.566 00(5)		
c (Å)	8.470 14(9)	8.467 77(8)	8.453 45(7)	8.458 66(8)	8.452 65(9)	8.441 3(1)
Volume ($Å^3$)	262.307(3)	261.862(2)	261.403(2)	261.351(3)	130.478(1)	130.175(1)
Sm *z*	0.137 41(8)	0.138 38(7)	0.139 37(6)	0.138 96(7)	0.139 93(8)	0.1420(1)
B_{iso} ($Å^2$)	0.51(2)	0.26(1)	0.29(1)	0.18(1)	0.21(1)	0.29(1)
Occ.	0.99(1)	0.99(1)	0.99(1)	0.99(1)	1.00(1)	0.99(1)
O B_{iso} ($Å^2$)	0.12(4)	0.8(2)	0.19(4)	0.13(3)	0.9(3)	0.8(4)
Occ.	0.98(2)	0.96(2)	0.92(2)	0.87(1)	0.86(1)	0.82(2)
F B_{iso} ($Å^2$)		0.8(2)	0.19(4)	0.13(3)	0.9(3)	0.8(4)
Occ.		0.04(2)	0.08(2)	0.13(1)	0.14(1)	0.18(2)
Fe B_{iso} ($Å^2$)	0.35(4)	0.11(2)	0.22(2)	0.12(2)	0.17(2)	0.09(4)
Occ.	1.00(1)	1.01(1)	1.01(1)	1.02(1)	1.00(1)	1.01(1)
As *z*	0.661 2(2)	0.660 0(1)	0.659 7(1)	0.66 02(1)	0.661 2(1)	0.660 8(2)
B_{iso} ($Å^2$)	0.27(2)	0.21(2)	0.13(1)	0.13(2)	0.09(2)	0.04(2)
Occ.	1.02(1)	1.02(1)	1.02(1)	1.02(1)	0.99(1)	1.00(1)
R_{wp} (%)	7.90	6.89	7.17	7.52	7.33	8.27
R_{exp} (%)	6.11	4.87	5.70	5.91	5.93	5.86
Sm-As (Å)	3.258 0(7)(2×)	3.257 5(6) (2×)	3.254 9(5) (2×)	3.260 7(7) (2×)	3.247 0(7) (4×)	3.237 5(9) (4×)
	3.269 8(7) (2×)	3.267 4(6) (2×)	3.261 2(5) (2×)	3.254 4(7) (2×)		
Sm-O/F (Å)	2.286 0(3) (4×)	2.288 7(3) (4×)	2.292 1(3) (4×)	2.289 9(3) (4×)	2.293 1(4) (4×)	2.300 4(4) (4×)
Fe-As (Å)	2.394 7(7) (4×)	2.388 2(6) (4×)	2.385 1(5) (4×)	2.387 0(7) (4×)	2.390 8(7) (4×)	2.387 1(9) (4×)
Fe-Fe (Å)	2.775 53(2) (2×)	2.774 68(2) (2×)	2.776 70(3) (2×)	2.775 55(3) (2×)	2.778 16(2) (4×)	2.776 80(2) (4×)
	2.789 42(2) (2×)	2.786 32(2) (2×)	2.784 15(3) (2×)	2.783 00(3) (2×)		
Fe-As-Fe (°)	110.49(5) (2×)	110.83(4) (2×)	111.04(4) (2×)	110.84(5) (2×)	110.50(5) (2×)	110.68(6) (2×)
	70.83(2) (2×)	71.03(2) (2×)	71.19(2) (2×)	71.10(2) (2×)	71.04(2) (4×)	71.13(3) (4×)
	71.24(3) (2×)	71.37(2) (2×)	71.42(2) (2×)	71.318(2) (2×)		
Sm-O/F-Sm (°)	118.78(3) (2×)	118.42(3) (2×)	118.13(2) (2×)	118.23(3) (2×)	117.90(3) (2×)	117.20(3) (2×)
	104.81(1) (2×)	105.01(1) (2×)	105.20(2) (2×)	105.16(1) (2×)	105.43(2) (4×)	105.75(2) (4×)
	105.24(1) (2×)	105.38(1) (2×)	105.44(1) (2×)	105.40(1) (2×)		

[a] *P*4/*nmm*: Sm on 2*c* (1/4, 1/4, *z*), Fe on 2*b* (3/4, 1/4, 1/2), O/F on 2*a* (3/4, 1/4, 0), As on 2*c* (1/4, 1/4, *z*).
[b] *Cmma*: Sm on 4*g* (0, 1/4, *z*), Fe on 4*b* (1/4, 0, 1/2), O/F on 4*a* (1/4, 0, 0), As on 4*g* (0, 1/4, *z*).

IV. DISCUSSION

The most prominent point arising from the results of the present structural refinements as a function of both temperature and composition is the survival of the orthorhombic crystal symmetry in $SmFeAsO_{1-x}F_x$ well beyond the onset of superconductivity. Crossing the metal-to-superconductor boundary at $x \sim 0.07$ is not accompanied by the complete suppression of the orthorhombic-to-tetragonal structural phase transition and, as for both x=0.10 and 0.12 compositions studied here $T_s > T_c$, both superconducting phases are orthorhombically distorted (Fig. 4). Although with increasing x T_s is shifting continuously to lower temperature values, the tetragonal symmetry in the superconducting state does not appear until well into the T_c versus x superconducting dome at x=0.15.

At first sight, given that T_c in the $SmFeAsO_{1-x}F_x$ family increases smoothly between $x \sim 0.07$ and 0.20, it may appear that the orthorhombic-to-tetragonal crossover is not reflected

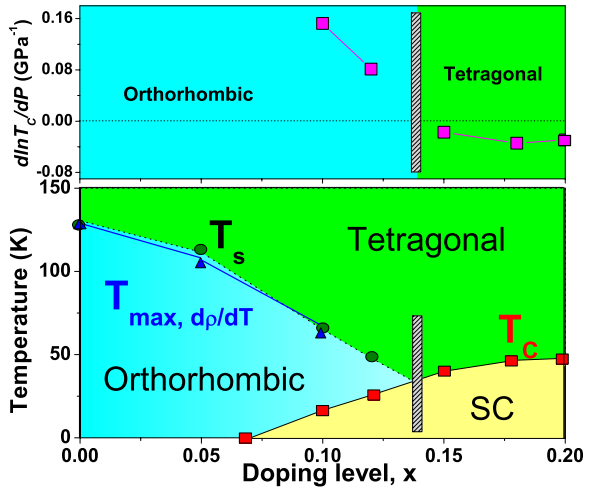

FIG. 4. (Color online) Structural and electronic phase diagrams of the $SmFeAsO_{1-x}F_x$ family. The red squares mark the superconducting transition temperatures T_c (Ref. 17), the green circles mark the tetragonal-to-orthorhombic structural transition T_s, and the blue triangles mark the temperature at which the first derivative of the resistivity with respect to temperature $d\rho/dT$ (Ref. 10) displays a maximum, $T_{\max,d\rho/dT}$ (bottom panel). The top panel shows the doping level dependence of the pressure coefficient of T_c, $d \ln T_c/dP$ (Ref. 17). The shaded bars near $x \sim 0.14$ mark the boundary for different behavior of the temperature-dependent resistivity (Ref. 10).

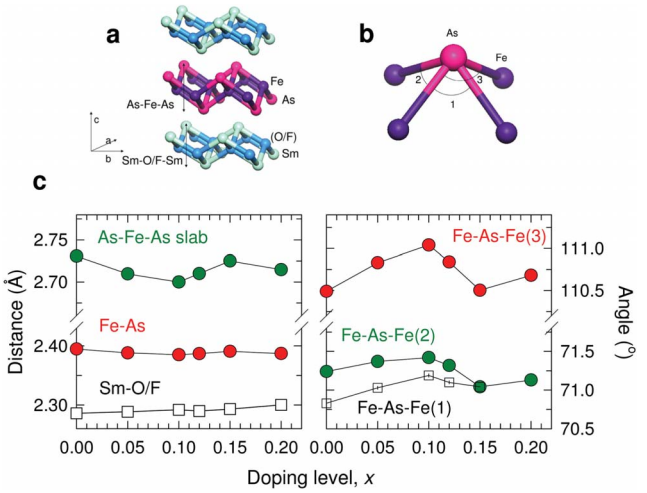

FIG. 5. (Color online) Structural parameters of the $SmFeAsO_{1-x}F_x$ family as a function of doping. (a) Schematic diagram of the crystal structure of $SmFeAsO_{1-x}F_x$. (b) Geometry of the $AsFe_4$ units and definition of the three (two) distinct Fe-As-Fe bond angles for the orthorhombic (tetragonal) crystal structure. (c) Doping dependence of selected bond distances and angles at 20 K. Error bars are smaller than the size of the symbols.

in the electronic properties despite the clear signature of the structural transformation in the temperature dependence of the resistivity (T_s coincides with the temperature $T_{\max}$ at which the first derivative of the temperature-dependent resistivity $d\rho/dT$ shows a maximum; Fig. 4) and in the renormalization of the bonding interactions within the conducting Fe-As slabs that accompany it (*vide infra*). However, here we recall two additional significant experimental observations already established for the $SmFeAsO_{1-x}F_x$ family that point toward the existence of a criticality hidden under the smoothly shaped superconducting dome at a doping level, $x \sim 0.14$: (i) the temperature dependence of the resistivity is linear at high temperatures (low temperatures just above T_c) for $x < 0.14$ ($x > 0.14$); this differing temperature evolution is accompanied by a drop in carrier density as observed by the pronounced rise in the Hall coefficient;[10] (ii) the superconducting response to pressure is drastically different for compositions straddling the $x \sim 0.14$ doping level (top panel of Fig. 4); while for $x < 0.14$ the pressure coefficient $\partial \ln T_c/\partial P$ of $SmFeAsO_{1-x}F_x$ is strongly positive, it switches sharply to negative at $x > 0.14$.[17] The observation that these pronounced anomalies in the electronic properties coincide exactly with the crossover from orthorhombic ($x < 0.14$) to tetragonal ($x > 0.14$) symmetry for the superconducting phase points toward a key role played by the structural order in determining the bonding interactions within the conducting Fe-As slabs and the electronic properties of the $SmFeAsO_{1-x}F_x$ superconductors.

The existence of a structural phase transition within the superconducting dome contrasts sharply with the absence of any reported coexistence of Néel magnetic order and superconductivity in the iron oxyarsenides. For instance, powder neutron-diffraction studies on the $CeFeAsO_{1-x}F_x$ family[9] have provided evidence that the magnetic SDW long-range order in the parent material is rapidly suppressed upon doping and disappears at a doping level $x \sim 0.06$ just before superconductivity emerges. The observed experimental phenomenology is reminiscent of recent theoretical work which has interpreted the tetragonal-to-orthorhombic phase transition as that to an electron nematic phase.[20,21] In analogy with the high-T_c cuprates,[22] while the Néel state does not coexist with superconductivity, other ordered states, such as Ising nematic states, can coexist with superconductivity and vanish at quantum critical points under the superconducting domes. Given the experimentally observed criticality in the structural, electronic, and conducting properties at $x \sim 0.14$ revealed for the $SmFeAsO_{1-x}F_x$ family here, it will be intriguing to search for effects of magnetic origin and establish the magnetic response of the normal state in the fluorine-doped rare-earth iron oxyarsenide families well beyond the compositional onset for superconductivity.

Finally, Fig. 5 shows the doping dependence at 20 K of selected crystallographic bond distances and angles. Gradual substitution of oxide by fluoride ions in the charge-reservoir Sm-O slab is accompanied by a gradual increase in the Sm-O/F distances. Focusing on the conducting Fe-As layer, we find that the thickness of the As-Fe-As slab [Fig. 5(a)] shows a clear discontinuity in the vicinity of the orthorhombic-to-tetragonal structural crossover at $x \sim 0.12$. This anomalous response is even more clearly evident in the x dependence of the Fe-As-Fe angles of the $AsFe_4$ pyramidal units [Fig. 5(b)]. These initially show a gradual increase in the orthorhombic phase as the doping level x increases. However, the suppression of the structural transition and the stabilization of the tetragonal phase at $x = 0.15$ is accompanied by a well-defined reduction in the magnitude of the Fe-As-Fe angles. As the

geometry of the $AsFe_4$ units [Fig. 5(b)] sensitively controls both the Fe near- and next-near-neighbor exchange interactions[23] and the width of the electronic conduction band,[9,24] the structural discontinuities near the critical composition $x \sim 0.14$ should be related with the observed electronic anomalies well within the superconducting dome.

V. CONCLUSION

In conclusion, we have found that there is a structural phase transition hidden well within the superconductivity phase diagram of the $SmFeAsO_{1-x}F_x$ family. This shows that the strong doping dependence of the magnetic long-range order which disappears before the onset of superconductivity is not reflected in the response of the structure. The orthorhombically distorted superconducting phases may be related to the electron nematic phases identified by theory, raising the question of the presence of incipient or fluctuating magnetic order well beyond the onset of superconductivity. The suppression of the tetragonal-to-orthorhombic phase transition near $x \sim 0.14$ coincides with well-defined anomalies in the electronic and conducting properties and in the pressure response of the superconducting transition of $SmFeAsO_{1-x}F_x$, revealing an intimate link between crystal and electronic structures in the iron oxyarsenide superconductors.

Note added. The key role played by the low-temperature orthorhombic structure in defining the electronic properties of the $SmFeAsO_{1-x}F_x$ family has been also demonstrated by muon spin-relaxation measurements,[25] which show that static magnetism persists well into the superconducting regime with the observed magnetic behavior mirroring exactly our established structural phase diagram. Moreover, magnetoresistance measurements on $SmFeAsO_{1-x}F_x$ (Ref. 26) find that an abrupt change in the magnetoresistance occurs around the structural crossover doping level of $x=0.15$. Finally, our results have now been confirmed for the related $LaFeAsO_{1-x}F_x$ and $CeFeAsO_{1-x}F_x$ systems for compositions over the more limited ranges of F doping levels of $0 \leq x \leq 0.08$ and $0 \leq x \leq 0.10$, respectively,[9,27] where it was also found that orthorhombic symmetry survives into the superconducting regime.

ACKNOWLEDGMENTS

We thank the ESRF for access to the synchrotron x-ray facilities. This work is partially supported by the Nature Science Foundation of China and the Ministry of Science and Technology of China.

*serena.margadonna@ed.ac.uk; k.prassides@durham.ac.uk

[1] Y. Kamihara, T. Watanabe, M. Hirano, and H. Hosono, J. Am. Chem. Soc. **130**, 3296 (2008).
[2] X. H. Chen, T. Wu, G. Wu, R. H. Liu, H. Chen, and D. F. Fang, Nature (London) **453**, 761 (2008).
[3] G. F. Chen, Z. Li, D. Wu, G. Li, W. Z. Hu, J. Dong, P. Zheng, J. L. Luo, and N. L. Wang, Phys. Rev. Lett. **100**, 247002 (2008).
[4] Z. A. Ren, J. Yang, W. Lu, W. Yi, G. C. Che, X. L. Dong, L. L. Sun, and Z. X. Zhao, Europhys. Lett. **82**, 57002 (2008).
[5] P. Cheng, L. Fang, H. Yang, X. Zhu, G. Mu, H. Luo, Z. Wang, and H. H. Wen, Sci. China, Ser. G **51**, 719 (2008).
[6] Z. A. Ren, G. C. Che, X. L. Dong, J. Yang, W. Lu, W. Yi, X. L. Shen, Z. C. Li, L. L. Sun, F. Zhou, and Z. X. Zhao, Europhys. Lett. **83**, 17002 (2008).
[7] C. de la Cruz, Q. Huang, J. W. Lynn, J. Li, W. Ratcliff, J. L. Zarestky, H. A. Mook, G. F. Chen, J. L. Luo, N. L. Wang, and P. Dai, Nature (London) **453**, 899 (2008).
[8] J. Dong, H. J. Zhang, G. Xu, Z. Li, G. Li, W. Z. Hu, D. Wu, G. F. Chen, X. Dai, J. L. Luo, Z. Fang, and N. L. Wang, Europhys. Lett. **83**, 27006 (2008).
[9] J. Zhao, Q. Huang, C. de la Cruz, S. Li, J. W. Lynn, Y. Chen, M. A. Green, G. F. Chen, G. Li, Z. Li, J. L. Luo, N. L. Wang, and P. Dai, Nature Mater. **7**, 953 (2008).
[10] R. H. Liu, G. Wu, T. Wu, D. F. Fang, H. Chen, S. Y. Li, K. Liu, Y. L. Xie, X. F. Wang, R. L. Yang, L. Ding, C. He, D. L. Feng, and X. H. Chen, Phys. Rev. Lett. **101**, 087001 (2008).
[11] L. Boeri, O. V. Dolgov, and A. A. Golubov, Phys. Rev. Lett. **101**, 026403 (2008).
[12] C. Cao, P. J. Hirschfeld, and H. P. Cheng, Phys. Rev. B **77**, 220506(R) (2008).
[13] X. Dai, Z. Fang, Y. Zhou, and F. C. Zhang, Phys. Rev. Lett. **101**, 057008 (2008).
[14] F. Ma and Z. Y. Lu, Phys. Rev. B **78**, 033111 (2008).
[15] T. Y. Chen, Z. Tesanovic, R. H. Liu, X. H. Chen, and C. L. Chien, Nature (London) **453**, 1224 (2008).
[16] T. Nomura, S. W. Kim, Y. Kamihara, M. Hirano, P. V. Sushko, K. Kato, M. Takata, A. L. Shluger, and H. Hosono, Supercond. Sci. Technol. **21**, 125028 (2008).
[17] Y. Takabayashi, M. T. McDonald, D. Papanikolaou, S. Margadonna, G. Wu, R. H. Liu, X. H. Chen, and K. Prassides, J. Am. Chem. Soc. **130**, 9242 (2008).
[18] A. C. Larsen and R. B. von Dreele, GSAS software, Los Alamos National Laboratory Report No. LAUR 86–748.
[19] The calculated, observed, and difference profiles of the Rietveld refinements for $SmFeAsO_{1-x}F_x$ ($x=0.05$, 0.12, and 0.15) at 20 K are included in the EPAPS Document No. E-PRBMDO-78-084845. For more information on EPAPS, see http://www.aip.org/pubservs/epaps.html.
[20] C. Fang, H. Yao, W.-F. Tsai, J. P. Hu, and S. A. Kivelson, Phys. Rev. B **77**, 224509 (2008).
[21] C. Xu, M. Müller, and S. Sachdev, Phys. Rev. B **78**, 020501(R) (2008).
[22] S. A. Kivelson, I. P. Bindloss, E. Fradkin, V. Oganesyan, J. Tranquada, A. Kapitulnik, and C. Howald, Rev. Mod. Phys. **75**, 1201 (2003).
[23] T. Yildirim, Phys. Rev. Lett. **101**, 057010 (2008).
[24] T. M. McQueen, M. Regulacio, A. J. Williams, Q. Huang, J. W. Lynn, Y. S. Hor, D. V. West, M. A. Green, and R. J. Cava, Phys. Rev. B **78**, 024521 (2008).
[25] A. J. Drew, C. Niedermayer, P. J. Baker, F. L. Pratt, S. J. Blun-

dell, T. Lancaster, R. H. Liu, G. Wu, X. H. Chen, I. Watanabe, V. K. Malik, A. Dubroka, M. Roessle, K. W. Kim, C. Baines, and C. Bernhard, arXiv:0807.4876 (unpublished).

[26] S. C. Riggs, J. B. Kemper, Y. Jo, Z. Stegen, L. Balicas, G. S. Boebinger, F. F. Balakirev, A. Migliori, H. Chen, R. H. Liu, and X. H. Chen, arXiv:0806.4011 (unpublished).

[27] Q. Huang, J. Zhao, J. W. Lynn, G. F. Chen, J. L. Luo, N. L. Wang, and P. Dai, Phys. Rev. B **78**, 054529 (2008).